FOUNDATIONS ADVANCES

ISSN 2053-2733

A simple formula for determining nanoparticle size distribution by combining small-angle X-ray scattering and diffraction results

Sérgio L. Morelhão[a]* and Stefan W. Kycia[b]*

[a]Institute of Physics, University of São Paulo, São Paulo, SP, Brazil, and [b]Department of Physics, University of Guelph, Guelph, ON, Canada. *Correspondence e-mail: morelhao@if.usp.br, skycia@uoguelph.ca

Received 25 April 2022
Accepted 13 July 2022

Edited by I. A. Vartaniants, Deutsches Electronen-Synchrotron, Germany

Keywords: nanocrystalline materials; nanoparticle size distribution; X-ray scattering and diffraction; Scherrer equation; Guinier approximation.

X-ray scattering and diffraction phenomena are widely used as analytical tools in nanoscience. Size discrepancies between the two phenomena are commonly observed in crystalline nanoparticle systems. The root of the problem is that each phenomenon is affected by size distribution differently, causing contrasting shifts between the two methods. Once understood, the previously discrepant results lead to a simple formula for obtaining the nanoparticle size distribution.

1. Introduction

Advances in nanoscience have demanded accurate measurements of particle size and size distribution as many physical and chemical properties of nanoparticle (NP) systems are size related (Borchert *et al.*, 2005; Keshari & Pandey, 2008; Grassian, 2008; Schwung *et al.*, 2014; Schmidt *et al.*, 2016; Clarke *et al.*, 2018; Kabir *et al.*, 2022). In the search for size determination methods, a simple but essential question is recurrent in X-ray analysis of polydisperse systems of crystalline NPs (Ingham, 2015; Gamez-Mendoza *et al.*, 2017; Freitas Cabral *et al.*, 2020; Kaduk *et al.*, 2021). In the wide-angle X-ray scattering (WAXS) region, what parameter of the particle size distribution (PSD) is determined by the diffraction peak width? Although there are general approaches describing how the diffraction peak line profiles are affected by size distribution (Scardi & Leoni, 2001; Leoni & Scardi, 2004; Cervellino *et al.*, 2005; Leonardi *et al.*, 2022), an explicit and direct answer to the above-mentioned question has been obscured by the mathematical formalism of more than 100 years of X-ray crystallography, as well summarized in Chapter 5.1 of the most recent volume of *International Tables for Crystallography*, Volume H (Leoni, 2019). The answer is the X-ray diffraction (XRD) peak width is defined by the median value $L_{\rm xrd}$ of the fourth moment integral of the PSD. It is valid as long as the maximum height of the diffraction peak follows a proportionality relationship with the NP size to the fourth power (Jones, 1938; Valério *et al.*, 2020). In other words, the diffraction peak width Δq obeys the Scherrer equation as stated in $\Delta q\, L_{\rm xrd} = \kappa_{\rm d}$ where the constant $\kappa_{\rm d}$ depends on NP shape (Scherrer, 1918).

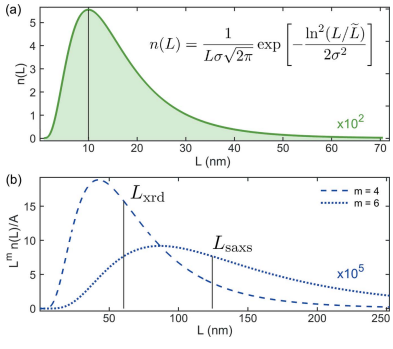

In the small-angle X-ray scattering (SAXS) region, the maximum intensity of scattering also follows a proportionality relationship with the size, but in this case with the NP size to the sixth power (Debye, 1915; Guinier & Fournet, 1955). Consequently, particle size determination in the SAXS region is dictated by the median value $L_{\rm saxs}$ of the sixth moment integral of the PSD. A measure of the radius of gyration $R_{\rm g}$ within the Guinier approximation (Guinier, 1939) has been

understood as a measure of $L_{saxs} = \zeta R_g$ where ζ is a value defined by the NP shape only. Depending on the experimental SAXS configuration, such as the ultra-SAXS configuration capable of detecting contributions of large NPs above 100 nm in general, it is also possible to measure the actual width Δq of scattering around the direct beam (Chapman *et al.*, 1997; Antunes *et al.*, 2006; Morelhão *et al.*, 2010; Ilavsky *et al.*, 2018). In this case, an analogous Scherrer equation approach, that is $\Delta q\, L_{saxs} = \kappa_s$, can be applied to obtain L_{saxs}, although the constant κ_s is slightly different than the one used for diffraction peaks in the WAXS region.

2. Results and discussion

Both κ_d and κ_s constants have the same values as those calculated for monodisperse systems (Appendix *A*). For instance, spherical NPs have $\kappa_d = 6.96$, corresponding to the well known Scherrer equation shape factor $K = \kappa_d/2\pi = 1.11$ (Patterson, 1939; Warren, 1990), while $\kappa_s = 7.26$ as determined from the analytical expression of the SAXS intensity curve for spheres. In polydisperse systems of spherical NPs, $L_{xrd} = 6.96/\Delta q$ stands for the XRD diameter value obtained from the diffraction peak width Δq (in reciprocal-space units), and $L_{saxs} = 7.26/\Delta q$ stands for the SAXS diameter value obtained by measuring the full width at half-maximum (FWHM) of the scattering peak around $q = 0$. For any other NP shape, numerical methods based on the Debye scattering equation can be used to compute exact values of the κ_s and κ_d constants (Farrow & Billinge, 2009; Cervellino *et al.*, 2015; Scardi & Gelisio, 2016; Leonardi *et al.*, 2022). In non-spherical NPs, κ_d can vary from one diffraction peak to another as in the case of cubic NPs where $\kappa_s = 5.64$ and the κ_d value falls in the range from 5.2 to 5.6, depending on the chosen diffraction peak and crystallographic orientation of the NP facets.

Although proper sample preparation and instrumental corrections are needed for size measurements in the SAXS and WAXS regions, we draw attention to the different weighting of the PSD by each one of these methods. It implies that XRD and SAXS size results will agree with each other as long as the PSD is narrow enough that median values of the fourth and sixth moment integrals are indistinguishable within their experimental errors. For systems of single-crystalline NPs, these two size values can be combined to determine two parameters of the size distribution probability function: specifically, the most probable size (mode) and the size dispersion or width of the size distribution. Numerical solutions are always feasible for any PSD function, requiring the median values of the momentum integrals to be plotted as a function of the mode and width of the size distribution. In the particular case of one of the most suitable probability functions for size distribution, that is the log-normal function (Kiss *et al.*, 1999), the median value of the *m*th moment integral has the analytical solution of $L_m = L_0 \exp[(m+1)\sigma^2]$ given in terms of the mode L_0 and the standard deviation in log-scale σ as the size dispersion parameter. Thus, the size values from XRD and SAXS measurements are $L_{xrd} = L_4 = L_0 \exp(5\sigma^2)$ and $L_{saxs} = L_6 = L_0 \exp(7\sigma^2)$, respectively. They lead to a simple equation for the size dispersion,

$$\sigma^2 = -\frac{1}{2}\ln\left(\frac{L_{xrd}}{L_{saxs}}\right), \qquad (1)$$

as well as an equally simple equation for the mode,

$$L_0 = L_{xrd}\exp(-5\sigma^2) = L_{saxs}\exp(-7\sigma^2). \qquad (2)$$

In systems where the size difference between SAXS and XRD results can be resolved, as for instance the case illustrated in Fig. 1 where $L_{saxs} \simeq 2L_{xrd}$, the size dispersion is quantifiable through equation (1), and the σ value thus obtained allows the PSD mode to be estimated by equation (2). On the other hand, a relatively small size dispersion parameter $\sigma = 0.1$ produces $L_{saxs} = 1.02L_{xrd}$ according to equation (1). As this 2% difference between SAXS and XRD results is very difficult to detect experimentally, size distributions for which $\sigma < 0.1$ are below the resolution of this method. For crystalline NP systems, comparing SAXS and XRD size measurements in this way can be very useful. Obtaining indistinguishable values for L_{saxs} and L_{xrd} allows one to prove that the NPs are single nanocrystals and the system is monodisperse ($\sigma < 0.1$). When $L_{saxs} > L_{xrd}$ there are a few possible situations – for example, a polydisperse system of single nanocrystals for which $\sigma > 0.1$, and in this case equations (1) and (2) can be applied to determine the size distribution. Otherwise, the NPs are multi-grains or may contain non-diffracting material.

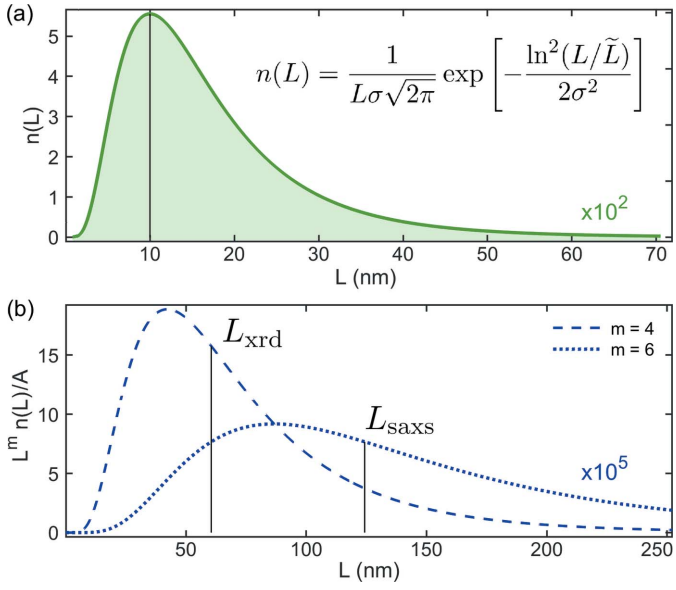

Figure 1
(*a*) Log-normal probability distribution function $n(L)$ for NP size L. Size dispersion parameter $\sigma = 0.6$ and mode $L_0 = 10$ nm. $\widetilde{L} = L_0\exp(\sigma^2)$. (*b*) Unit area curves of the fourth and sixth moments of the probability function in (*a*), $A = \int_0^\infty L^m n(L)\,dL$, showing medians $L_m = L_0\exp[(m+1)\sigma^2]$ (vertical lines) as the XRD ($m = 4$) and SAXS ($m = 6$) size values where $L_{saxs} \simeq 2L_{xrd}$.

3. Conclusions

In summary, the scattering and diffraction results of particle size agree with each other exclusively for samples with narrow size dispersion. It implies that, to explain the difference in size values from both methods, size dispersion is a hypothesis that must be considered. Being able to determine size distribution by combining scattering and diffraction methods is an asset to advanced X-ray instruments capable of simultaneously performing SAXS and WAXS (Ilavsky *et al.*, 2018; Smith *et al.*, 2021; Shih *et al.*, 2022). *In situ* studies of the evolution of PSD during crystallization processes and chemical reactions are feasible by exploiting such instruments.

APPENDIX *A*
A general property of peak functions

A peak profile function $P_L(q)$ with maximum height $P_L(q_0) = AL^m$ and FWHM $\Delta q = \kappa L^{-1}$ leads to the weighted peak

$$I(q) = \int P_L(q) n(L)\, \mathrm{d}L \qquad (3)$$

according to the probability distribution function $n(L)$ for parameter L. At the half-maximum of $I(q)$ where $\Delta q = q_{\rm right} - q_{\rm left}$,

$$I(q_0 - q_{\rm left}) = I(q_0 + q_{\rm right}) = \tfrac{1}{2}\int P_L(q_0) n(L)\, \mathrm{d}L = A \int_0^{L^*} L^m n(L)\, \mathrm{d}L. \qquad (4)$$

For narrow distribution functions, it is straightforward to see that $\Delta q L^* = \kappa$. This relationship also holds for broad distributions as verified numerically for a variety of peak profile functions, probability distributions and m values. For instance, it is demonstrated in Fig. 2(*a*) by using $P_L(q)$ as the analytical expression of the SAXS curve for spheres of diameter L, and $n(L)$ as the log-normal function, inset of Fig. 1(*a*). In this case, $m = 6$ and the values of $L^* = \kappa/\Delta q$ follow very closely the predicted behavior of the median value $L_6 = L_0 \exp(7\sigma^2)$, as compared in Fig. 2(*b*). Therefore, by using the same constant κ that determines the FWHM of the peak function $P_L(q)$, a measure of the weighted peak FWHM leads to the median value L_m of the mth momentum integral of the probability distribution function $n(L)$. The validity of this statement for any combination of peak profile and distribution functions can always be confirmed through equation (4).

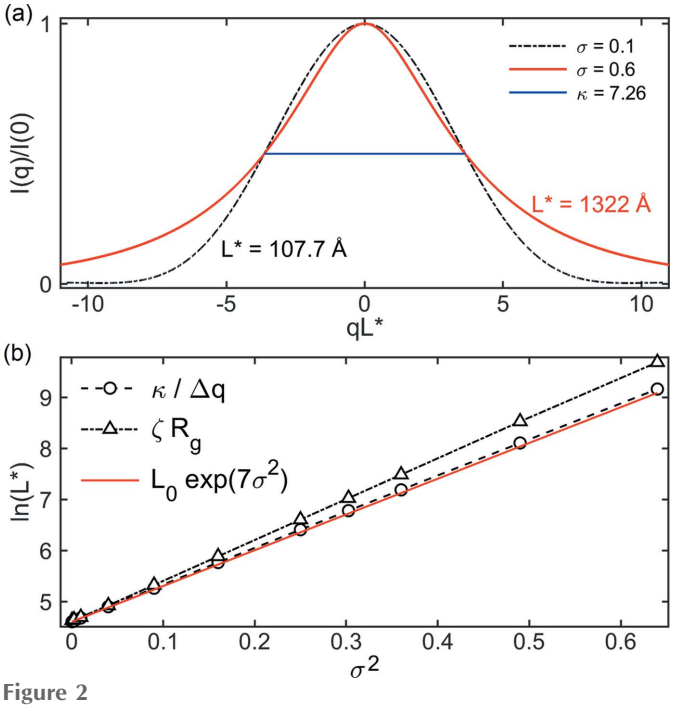

Figure 2
(*a*) SAXS curves for dilute systems of spheres with log-normal size distributions of mode $L_0 = 100$ Å in diameter: $I(q)$ as in equation (3), σ as in Fig. 1(*a*) (inset), and $P_L(q) = [(\sin(u) - u\cos(u))/u^3]^2 L^6$ where $u = qL/2$. As a function of $qL^* = \kappa(q/\Delta q)$, both curves have width $\kappa = 7.26$. (*b*) Comparison of L^* values from the weighted SAXS curves, obtained as $\kappa/\Delta q$ and $\zeta R_{\rm g}$, with the expected median value $L_0 \exp(7\sigma^2)$. $\zeta = (20/3)^{1/2}$ is the diameter/radius-of-gyration ratio of a sphere. From each weighted SAXS curve, $R_{\rm g} = -3\ln[I(q)/I(0)]/q^2$ in the limit of $q \to 0$.

Funding information

Funding for this research was provided by: Fundação de Amparo à Pesquisa do Estado de São Paulo (grant No. 2019/01946-1); Conselho Nacional de Desenvolvimento Científico e Tecnológico (grant No. 310432/2020-0); Natural Sciences and Engineering Research Council of Canada.

References

Antunes, A., Safatle, A. M. V., Barros, P. S. M. & Morelhão, S. L. (2006). *Med. Phys.* **33**, 2338–2343.
Borchert, H., Shevchenko, E. V., Robert, A., Mekis, I., Kornowski, A., Grübel, G. & Weller, H. (2005). *Langmuir*, **21**, 1931–1936.
Cervellino, A., Frison, R., Bertolotti, F. & Guagliardi, A. (2015). *J. Appl. Cryst.* **48**, 2026–2032.
Cervellino, A., Giannini, C., Guagliardi, A. & Ladisa, M. (2005). *Phys. Rev. B*, **72**, 035412.
Chapman, D., Thomlinson, W., Johnston, R. E., Washburn, D., Pisano, E., Gmür, N., Zhong, Z., Menk, R., Arfelli, F. & Sayers, D. (1997). *Phys. Med. Biol.* **42**, 2015–2025.
Clarke, G., Rogov, A., McCarthy, S., Bonacina, L., Gun'ko, Y., Galez, C., Le Dantec, R., Volkov, Y., Mugnier, Y. & Prina-Mello, A. (2018). *Sci. Rep.* **8**, 10473.
Debye, P. (1915). *Ann. Phys.* **351**, 809–823.
Farrow, C. L. & Billinge, S. J. L. (2009). *Acta Cryst.* A**65**, 232–239.
Freitas Cabral, A. J., Valério, A., Morelhão, S. L., Checca, N. R., Soares, M. M. & Remédios, C. M. R. (2020). *Cryst. Growth Des.* **20**, 600–607.
Gamez-Mendoza, L., Terban, M. W., Billinge, S. J. L. & Martinez-Inesta, M. (2017). *J. Appl. Cryst.* **50**, 741–748.
Grassian, V. H. (2008). *J. Phys. Chem. C*, **112**, 18303–18313.
Guinier, A. (1939). *Ann. Phys.* **11**, 161–237.
Guinier, A. & Fournet, G. (1955). *Small-Angle Scattering of X-rays.* New York: John Wiley & Sons, Inc.
Ilavsky, J., Zhang, F., Andrews, R. N., Kuzmenko, I., Jemian, P. R., Levine, L. E. & Allen, A. J. (2018). *J. Appl. Cryst.* **51**, 867–882.
Ingham, B. (2015). *Crystallogr. Rev.* **21**, 229–303.
Jones, F. W. (1938). *Proc. R. Soc. Lond. A*, **166**, 16–43.
Kabir, I. I., Osborn, J. C., Lu, W., Mata, J. P., Rehm, C., Yeoh, G. H. & Ersez, T. (2022). *J. Appl. Cryst.* **55**, 353–361.

Kaduk, J. A., Billinge, S. J. L., Dinnebier, R. E., Henderson, N., Madsen, I., Černý, R., Leoni, M., Lutterotti, L., Thakral, S. & Chateigner, D. (2021). *Nat. Rev. Methods Primers*, **1**, 77.
Keshari, A. K. & Pandey, A. C. (2008). *J. Nanosci. Nanotechnol.* **8**, 1221–1227.
Kiss, L. B., Söderlund, J., Niklasson, G. A. & Granqvist, C. G. (1999). *Nanotechnology*, **10**, 25–28.
Leonardi, A., Neder, R. & Engel, M. (2022). *J. Appl. Cryst.* **55**, 329–339.
Leoni, M. (2019). *International Tables for Crystallography*, Vol. H, *Powder Diffraction*, 1st ed., ch. 5.1, pp. 524–537. Chester: International Union of Crystallography.
Leoni, M. & Scardi, P. (2004). *J. Appl. Cryst.* **37**, 629–634.
Morelhão, S. L., Coelho, P. G. & Hönnicke, M. G. (2010). *Eur. Biophys. J.* **39**, 861–865.
Patterson, A. L. (1939). *Phys. Rev.* **56**, 978–982.
Scardi, P. & Gelisio, L. (2016). *Sci. Rep.* **6**, 22221.
Scardi, P. & Leoni, M. (2001). *Acta Cryst.* A**57**, 604–613.
Scherrer, P. (1918). *Nachr. Ges. Wiss. Goettingen, Math.-Phys. Kl.* p. 98.
Schmidt, C., Riporto, J., Uldry, A., Rogov, A., Mugnier, Y., Dantec, R. L., Wolf, J.-P. & Bonacina, L. (2016). *Sci. Rep.* **6**, 25415.
Schwung, S., Rogov, A., Clarke, G., Joulaud, C., Magouroux, T., Staedler, D., Passemard, S., Jüstel, T., Badie, L., Galez, C., Wolf, J. P., Volkov, Y., Prina-Mello, A., Gerber-Lemaire, S., Rytz, D., Mugnier, Y., Bonacina, L. & Le Dantec, R. (2014). *J. Appl. Phys.* **116**, 114306.
Shih, O., Liao, K.-F., Yeh, Y.-Q., Su, C.-J., Wang, C.-A., Chang, J.-W., Wu, W.-R., Liang, C.-C., Lin, C.-Y., Lee, T.-H., Chang, C.-H., Chiang, L.-C., Chang, C.-F., Liu, D.-G., Lee, M.-H., Liu, C.-Y., Hsu, T.-W., Mansel, B., Ho, M.-C., Shu, C.-Y., Lee, F., Yen, E., Lin, T.-C. & Jeng, U. (2022). *J. Appl. Cryst.* **55**, 340–352.
Smith, A. J., Alcock, S. G., Davidson, L. S., Emmins, J. H., Hiller Bardsley, J. C., Holloway, P., Malfois, M., Marshall, A. R., Pizzey, C. L., Rogers, S. E., Shebanova, O., Snow, T., Sutter, J. P., Williams, E. P. & Terrill, N. J. (2021). *J. Synchrotron Rad.* **28**, 939–947.
Valério, A., Morelhão, S. L., Cabral, A. J. F., Soares, M. M. & Remédios, C. M. R. (2020). *MRS Adv.* **5**, 1585–1591.
Warren, B. E. (1990). *X-ray Diffraction.* New York: Dover Publications.